Facultad de Ciencias e Ingeniería
sección
Física

Results Report - February 2023

# Modificación del código fuente de MadAnalysis5 para lograr una comparación de datos reconstruidos con reales y Ejecución de FastJet para una asignación de jets

*Walter Rodríguez,*
*Danilo Zegarra*

supervised by
Joel Jones-Perez

**Acknowledgements**

We are greatly thankful to our advisor, Dr. Joel Jones-Perez, for the fruitful feedback and advises given in this project. We also thank the *Facultad de Ciencias e Ingeniería* (FCI) from PUCP for the funding that made posible for us to do this research.

**Abstract**

*In collider physics simulations, it is valuable to compare the Monte Carlo data to the reconstructed information. This can be achieved, for certain quantities, with* `MadAnalysis 5`*, a software whose importance relies on extracting this information and to impose cuts to an event to see if the expected results would be observed if made in real colliders. There is a major flaw and that is that it can not gather the information for displaced vertices and the quantities of interest for jets. This information is crucial for many purposes but for our context is needed to study heavy neutrino decay signals. This work details the instructions modify the source code to collect these two pieces of data using* `MadAnalysis 5`*.*

**Keywords**

Long live particles, Heavy neutrino, Type-I Seesaw model, Displaced vertices, Jet algorithm

# Contents

# 1 Introduction

The Standard Model of elementary particles (SM) is a theory that describes the strong, weak, and electromagnetic interactions. Despite its great theoretical and experimental success, there are still many unknowns to be resolved. One of these is the mass of neutrinos. In this model, neutrinos are massless particles, however, this feature has been refuted by neutrino oscillation experiments. The Seesaw mechanism is a possible extension that could explain this. To do this, it adds right-hand neutrinos to the SM that allow the generation of both Dirac and Majorana mass terms. This model, additionally, explains the suppression of the mass of the SM neutrinos concerning the other fermions. This motivates the search for heavy neutrinos in colliders such as the LHC through proton-proton collisions.

The Monte Carlo simulator `MadGraph5_aMC@NLO` allows for the study of events produced in high-energy colliders using theoretical models such as the Seesaw model at the LHC. With the `MadAnalysis 5` program, experimental cuts can be imposed to explore whether a hypothetical theoretical proposal would have observable results in real colliders. In this context, these simulators represent important study tools for finding favorable channels for signals that could show heavy neutrino results in colliders such as the LHC.

This work shows the use of these programs to simulate the collider signatures of the Type-I Seesaw model. This is a particular case of Seesaw where the hierarchy of scales between the Dirac and Majorana masses is larger than the electroweak scale. In this context we will focus on the case where these neutrinos are long-lived particles (LLP) where their decays can be detected via displaced vertices. In contrast, heavy neutrinos can also lead to the production of prompt charged leptons coming from the primary vertex. This is a reasonable way to search and discover this kind of neutrino. For this reason, it is important to notice that the displaced vertex method would be important not for discovering these neutrinos but for measuring their properties and correspondence with the model Type-I Seesaw.

Hadronization of quarks and gluons leads to a parton shower, where the particles multiply and form a stream of quarks and gluons. To relate the final state hadrons with the original partons, the concept of Jet is introduced, where the particles are collimated into a narrow cone as they move away from the interaction point. Since we will be interested in the decay of the heavy neutrino in $N \to \mu qq'$, we want to correctly associate the quarks with the jets. There are different algorithms for the jet reconstruction, in this report will be used the anti-$k_t$ jet algorithm that

will be presented in Section 2.5.

To achieve the correct analysis of displaced vertices and jet reconstruction, the objectives of this work are the following: modify the `MadAnalysis 5` code consistently so that the production point information for each particle of each event is available to the user at the Monte Carlo level and run FastJet externally but in parallel with `MadAnalysis 5` in order to achieve a jet assignment. The first objective is important to obtain the information of the displaced vertices and the second would allow the correct reconstruction of jets with more flexibility.

# 2 Theoretical Framework

The Standard Model of particle physics (SM) explains the three fundamental forces of the subatomic world: electromagnetic, weak nuclear, and strong nuclear. In addition, this theory describes the interaction and characteristics of two kinds of particles: bosons and fermions.

Fermions are characterized by obeying the Fermi-Dirac statistics. Additionally, they satisfy the Pauli exclusion principle. These particles possess a semi-integer spin and are conformed by quarks and leptons. These two last particles have in common the spin that is $\frac{1}{2}$. In the case of the leptons, there are charged and neutral. The charged are the electrons ($e$), muons ($\mu$) and taus ($\tau$) and the neutrals associated are the electron neutrino ($\nu_e$), muon neutrino ($\nu_\mu$) and tau neutrino ($\nu_\tau$). The neutrinos, as we will explain later, are of main interest in this work.

On the other hand, the bosons obey the Bose-Einstein statistic and have an integer spin. There are four types of bosons with spin 1: gluons ($g$), photons ($\gamma$), and the $Z$ and $W^\pm$ bosons. Each one of these is the mediator of the strong, electromagnetic, and electroweak forces respectively. There is also a boson with spin 0: the Higgs bosons ($h$). This particle, via the Brout-Englert-Higgs mechanism, gives masses to the other particles of the SM.

The SM only describes the 5% of the composition of the universe leaving open many questions. One of them is the possibility of the unification of the subatomic forces with the force of gravity. In this case, we are going to focus on another important problem: the neutrino masses. In the SM these particles must be massless. Nevertheless, this fact has been disproved by the neutrino oscillations experiments.

For this reason, it is crucial to find a theoretical explanation for the masses of these particles. One possibility would be to search for a new theory that could explain all the phenomena of the SM and also the neutrino masses. In contrast, there is another possibility: an extension of the

SM. In this case, the SM will be used as a starting point.

## 2.1 Seesaw Mechanism

This work will be focused on an extension of the SM that can explain the masses of neutrinos: Seesaw Mechanism [1–4]. If the model adds $N$ right-handed neutrinos ($\nu_R$) to the SM, then will be a Seesaw $3+N$. The next chapter will be explained a particular case: the Seesaw $1+1$ model a simple theoretical example.

A relevant question is how these Seesaw models can explain the neutrino masses. In general, when a right-handed neutrino is added, then it is possible to generate Majorana and Dirac mass terms. For the generation of these last terms, it is necessary to have an electroweak symmetry braking, which is an analogous procedure to obtain the masses terms of the leptons and quarks.

An important unsolved question in neutrino physics involves the big difference in the hierarchy of scales between the neutrinos and the other fermions. In the Seesaw model, this can be explained after the diagonalization of the mass matrix. This allows us to have an inverse relation between the SM neutrinos masses and the Majorana masses. Thus, if the Majorana masses are bigger, then the SM neutrino masses will be more suppressed [5].

Depending on the hierarchy of scales between the Dirac and Majorana masses, there could be different kinds of Seesaw models. On one hand, if this difference is almost zero, then the model corresponds to a mini-seesaw. On the other hand, if the difference is larger than the electroweak scale, then this corresponds to a Type-I Seesaw model [6].

This last model is of special interest because the possibility to test their implications in particle colliders such as the LHC and predict the existence of heavy neutrinos. These particles would be electrically neutral and would not be able to deposit their energy in the detectors.

If heavy neutrinos exist and are LLP, then there are two possible scenarios [7]. On one hand, if they are produced by the decay of the Higgs, then the signal could be obtain by displaced vertices. This signal could have an energetic lepton as a trigger, but this lepton would not be prompt.

Another possible production channel is via a virtual $W$, where it decays into a heavy neutrino and a lepton. In this case, the lepton associated with that vertex would be prompt. However, the lepton associated with the subsequent decay of the heavy neutrino would also be displaced. Thus, obtaining only one prompt charged lepton is not a prediction of the Seesaw model. For

example, if a $W$ is produced, it could decay into a SM neutrino and a prompt charged lepton.

### 2.1.1 Seesaw 1+1

As a first approach will introduce the most simple case of Seesaw model: Seesaw $1+1$ [8]. Here the case where there is only one SM neutrino with an arbitrary flavor will be analyzed.
This toy model will be useful for understanding the interaction between a right-handed neutrino $\nu_R$ with the neutrinos of the SM. Moreover, this will explain the big difference in the hierarchy of scales between the neutrinos and the other leptons. The Yukawa coupling of this model is the following:

$$\mathcal{L}_{\text{mass}} = f_\nu \overline{\nu_R} \phi l_L, \tag{1}$$

where $f_\nu$ is the Yukawa coupling constant, the Higgs bosson ($\phi$) is a doublet $SU(2)$ conformed by complex scalar fields:

$$\phi = \begin{pmatrix} \phi_\alpha \\ \phi_\beta \end{pmatrix} = \sqrt{\frac{1}{2}} \begin{pmatrix} \phi_1 + i\phi_2 \\ \phi_3 + i\phi_4 \end{pmatrix}$$

and $l_L$ represents a doublet $SU(2)$ conformed by an active neutrino $\nu_l$ and the respective lepton $l$ with the same flavor:

$$l_L = \begin{pmatrix} l \\ \\ \nu_l \end{pmatrix}$$

After a chiral symmetry breaking and giving a vacuum expectation value to $\phi$ it is possible to obtain a Dirac mass term. This process is done on an equal footing to the other fermions of the SM:

$$\mathcal{L}_{\text{mass}} = m \overline{\nu_R} \nu_L = f \overline{\nu_R} \nu_L \left\langle \phi^0 \right\rangle . \tag{2}$$

Additionally, because $\nu_R$ satisfies the Majorana condition:

$$\nu_R^c = \nu_R, \tag{3}$$

it is possible to obtain a Majorana mass term:

$$\mathcal{L}' = \frac{M}{2} \bar{\nu}_R^c \nu_R + \text{ h.c.} \tag{4}$$

In this way, the masses terms of this first example of Seesaw are defined by the contribution of both:

$$\mathcal{L} = f\overline{\nu_R}\nu_L \left\langle \phi^0 \right\rangle + \frac{M}{2}\overline{\nu_R^c}\nu_R + \text{ h.c.} \tag{5}$$

If the mass matrix of this lagrangian is diagonalized,

$$\mathcal{M} = \begin{pmatrix} 0 & m \\ m & M \end{pmatrix} \tag{6}$$

where $m = f\langle\phi^0\rangle$, it is possible to obtain:

$$m_{\nu_L} \simeq \frac{m^2}{M}, \tag{7}$$

for the limit where $M \gg \langle\phi^0\rangle$. This expression shows that because of the suppression that the SM neutrinos receive from the Majorana masses $M$, it is possible to explain why the neutrino masses are so small compared with the other leptons.

### 2.1.2 Type I Seesaw 3+2

This work will analyze the Type-I Seesaw scenario. This means that the hierarchy of scales between the Dirac and Majorana masses is larger than the electroweak scale as explained in section 2.1 .This will be done in the context of the 3+2 minimal model (MM). In contrast, there is also a 3+2 phenomenological model (PM). The main difference between them is the number of independent mass differences, mixing angles, and CP phases. In the case of the MM, this quantity is 4, 4 and 3 respectively. Meanwhile, in the PM it is 4, 9 and 5 [6].

The minimal model $3 + 2$ can be obtained by adding two heavy Majorana spinors $\nu_R$. These particles are singlets under gauge symmetries. They are identified as heavy sterile neutrinos and have a Majorana mass $M_R$. Additionally, they can couple with the active neutrinos of the SM thanks to the Yukawa coupling $Y_\nu$.

The most general renormalizable lagrangian of this model that include the right-handed singlet is the following: [9]:

$$\mathcal{L} = \mathcal{L}_{SM} - \sum_{a,s_i} \bar{l}_L^a Y^{as_i} \tilde{\phi} \nu_R^{s_i} - \sum_{s_i,s_j} \frac{1}{2} \bar{\nu}_R^{s_i c} M_N^{s_i s_j} \nu_R^{s_j} + \text{ h.c}, \tag{8}$$

where the index $a$ represent the active flavours $e, \mu, \tau$ and the indices $s_i, s_j = 1, 2$ to the two sterile neutrinos. Meanwhile, the Yukawa matrix $Y$ is $3 \times 2$ and $M_N$ is a two-dimensional symmetric matrix.

After the electroweak symmetry breaking of the lagrangian, it is possible to generate a Dirac mass from the coupling between $\nu_L$ and $\nu_R$. Consequently, the $5 \times 5$ neutrino mass matrix [7] can be obtained:

$$\mathcal{M}_\nu = \begin{pmatrix} 0 & m_Y \\ m_Y^T & M_N \end{pmatrix}, \tag{9}$$

where $M_N = \text{Diag}\,(M_1,\ \ M_2)$ and $m_Y$ is a matrix $3 \times 2$ which is defined by $(m_Y)_{\alpha i} = \nu(Y)_{\alpha i}/\sqrt{2}$. In this last definition, $\nu$ represent the vacuum expectation value.

In analogy with the Seesaw $1 + 1$, after the diagonalization can obtain a relation for the light neutrino matrix:

$$m_\nu \sim m_D^T M_R^{-1} m_D \tag{10}$$

This equation explains that the low mass of SM neutrinos is associated with the high mass of right-hand neutrinos. As will be shown later, this relation can change depending on the parametrization and the selected values of it.

There exists a matrix $U$ that can diagonalize the mass matrix of the neutrino such that:

$$\mathcal{M}_\nu = U^* \,\text{Diag}\,(0,\ \ m_2,\ \ m_3,\ \ M_1,\ \ M_2)\, U^\dagger, \tag{11}$$

with $m_2, m_3, M_1, M_2$ the mass eigenstates. It is possible to parameterize $U$ in four blocks [6] that represent the mixtures between the active components $a = (e,\ \ \mu,\ \ \tau)$, sterile $s = (s_1,\ \ s_2)$, light $l = (1,\ \ 2,\ \ 3)$ and heavy $h = (1,\ \ 2)$:

$$U_{5\times5} = \begin{pmatrix} (U_{al})_{3\times3} & (U_{ah})_{3\times2} \\ (U_{sl})_{2\times3} & (U_{sh})_{2\times2} \end{pmatrix} \tag{12}$$

with

$$\begin{aligned} &U_{al} = U_{PMNS} \begin{pmatrix} 1 & 0 \\ 0 & H \end{pmatrix}, \ \ U_{ah} = i U_{PMNS} \begin{pmatrix} 0 \\ H m_l^{1/2} R^\dagger M_h^{-1/2} \end{pmatrix}, \\ &U_{sl} = i \begin{pmatrix} 0 & \bar{H} M_h^{-1/2} R m_l^{1/2} \end{pmatrix}, \ \ U_{sh} = \bar{H}. \end{aligned} \tag{13}$$

where

$$H^{-2} = I + m_l^{1/2} R^\dagger M_h^{-1} R m_l^{1/2} \qquad \bar{H}^{-2} = I + M_h^{-1/2} R m_l R^\dagger M_h^{-1/2}. \tag{14}$$

In Eq. 13, $U_{PMNS}$ is a unitary matrix $3\times3$ that corresponds to the mixing matrix of the neutrinos in the limit where $H \to I$. For diagonal matrix we have the relation $M_h = \text{Diag}\,(M_1,\ M_2)$ with mostly sterile terms. Assuming that the neutrinos have a normal hierarchy (NH), we have $m_l = \text{Diag}\,(m_2,\ m_3) = \text{Diag}\left(\sqrt{\Delta m^2_{sol}},\ \sqrt{\Delta m^2_{atm}}\right)$ with most active terms. Finally, we have a complex orthogonal matrix $R$ that is parameterized as

$$R = \begin{pmatrix} \cos\left(\theta_{45} + i\gamma_{45}\right) & \sin\left(\theta_{45} + i\gamma_{45}\right) \\ -\sin\left(\theta_{45} + i\gamma_{45}\right) & \cos\left(\theta_{45} + i\gamma_{45}\right) \end{pmatrix}. \tag{15}$$

Analyzing the parameters of $R$, we observe that in the particular case where $|\gamma_{45}| \gtrsim 2 - 3$ the Eq. ( 15) can be expressed as:

$$R_{|\gamma_{45}|\gg1} = \begin{pmatrix} 1 & \pm i \\ \mp i & 1 \end{pmatrix} \cosh\gamma_{45} e^{\mp i\theta_{45}}. \tag{16}$$

Since we are interested in the terms $|U|^2$, then the global phase $\theta_{45}$ does not influence the phenomenology of the model. Thus, the important parameters of this model will be the two masses of the heavy neutrinos $M_1, M_2$ and the angle $\gamma_{45}$. In particular, considering the constraints given in [10, 11] and [12] we take: $M_1 = M_2$ =15 GeV and $\gamma_{45}$ =8. These orders in the masses $M_1$ and $M_2$ will allow to have a LLP regime; this is important if we want to study displaced vertices for the heavy neutrinos.

In search of simplifying the expressions for active-heavy mixes, we analyze the particular case where $H \sim I$. For the parameterization of $U$ made previously (NH) we have [13]:

$$\begin{aligned} U_{\ell4} \equiv (U_{ah})_{\ell1} &= \pm Z_\ell^{\text{NH}} \sqrt{\frac{m_3}{M_1}} \cosh\gamma_{45} e^{\pm i\theta_{45}}, \\ U_{\ell5} \equiv (U_{ah})_{\ell2} &= i Z_\ell^{\text{NH}} \sqrt{\frac{m_3}{M_2}} \cosh\gamma_{45} e^{\pm i\theta_{45}} \end{aligned} \tag{17}$$

where

$$Z_\ell^{\text{NH}} = (U_{\text{PMNS}})_{\ell3} \pm i\sqrt{\frac{m_2}{m_3}}\,(U_{\text{PMNS}})_{\ell2}\,. \tag{18}$$

Additionally, up to corrections of order $\mathcal{O}(m_3/M_j)$a relation between the Dirac mass matrices and the Yukawa terms can be obtained:

$$\begin{aligned}(m_D)_{\ell 1} &= \pm \left(Z_\ell^{\rm NH}\right)^* \sqrt{m_3 M_1}\cosh\gamma_{45} e^{\mp i\theta_{45}} \\ (m_D)_{\ell 2} &= -i \left(Z_\ell^{\rm NH}\right)^* \sqrt{m_3 M_2}\cosh\gamma_{45} e^{\mp i\theta_{45}}\end{aligned} \tag{19}$$

In the Eq. (19) it is observed that the term $\gamma_{45}$ generates an exponential enhancement for the Dirac terms, which does not occur in other Seesaw models as the Seesaw 1 + 1, where $m_D \sim \sqrt{m_i M_j}$ is the only possible relation.

In the case that $M_N < m_h$, where $m_h$ is the mass of the Higgs and $M_N$ the mass of the heavy neutrino, the *branching ratio* (BR) of $h \to nN$ will be the least suppressed concerning the BRs of $h \to nn$ and $h \to NN$ [14]. This happens because of the exponential enhancement in Eq.(17) that affects the active-heavy mixes.

The BR of the process $h \to n_i N_j$ is calculated in the paper [15] and has the form:

$$BR(h \to n_i N_j) = \frac{\Gamma(h \to n_i N_j)}{\Gamma_{SM} + \sum_{i,j}\Gamma(h \to n_i N_j)}, \tag{20}$$

with

$$\Gamma\left(h \to n_i N_j\right) = \frac{g^2}{32\pi}\frac{M_j^2}{m_W^2} m_h \left(1 - y_j^2\right)^2 |C_{ij}|^2 \tag{21}$$

where $m_W$ is the $W$ boson mass and $y_j = M_j/m_h$. For NH it can be obtained:

$$C_{lh} = i \begin{pmatrix} 0 \\ H^2 m_\ell^{1/2} R^\dagger M_h^{-1/2} \end{pmatrix}. \tag{22}$$

A relevant question is which of the three flavors will be the most probable in the decay of the heavy neutrino. Considering the Eq. 17 the most suppressed couple will be in the case of the electrons. This is due to the term $(U_{\rm PMNS})_{\ell 3}$ that is proportional to $\theta_{13}$. This last term is smaller than the others with different indices.

For this reason, muonic and tauonic decay are the most probable. However, due to the rapid decay of taus into jets in the detector and the difficulty in distinguishing between the two objects, this particle will not be analyzed in this report. Consequently, only the muonic decay channel will be analyzed in detail.

Thus, the decay channel that involves muons and quarks ($N \to \mu q q'$) is considered the most

probable and is represented by the diagram shown in Figure 1:

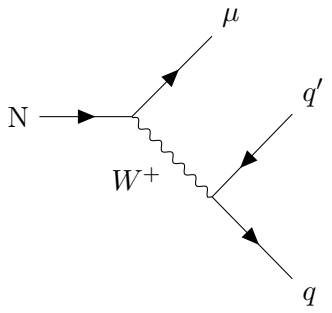


Figure 1: Feynman diagram of the main decay channel of the analyzed heavy neutrino $N \to \mu q q'$.

## 2.2 Large Hadron Collider (LHC)

The Large Hadron Collider (LHC) is a hadron accelerator and collider. It is composed of two rings that contain superconducting magnets. It was installed in 26.7 kilometers in circumference tunnel and was built between the years 1984 and 1989 [16].

His main objective was to discover the Higgs boson, a particle that gives mass to the $W$ and $Z$ bosons through electroweak symmetry breaking. The discovery was announced in 2012 in proton-proton collisions ($pp$) at an energy of the center of mass $\sqrt{s} = 7$ and 8 TeV. This was done with a significance of $5.0\sigma$ for a mass close to the 125 GeV [17, 18]. Additionally, this collider also searches for signals from BSMs, analyzing supersymmetry models and possibly dark matter candidates.

How was the Higgs detected in the LHC? For answering this question is important to know the difference between the production and detection of particles in the context of the LHC. The first is independent of the observer or instrument, it is a natural phenomenon that occurs in a certain coordinate of the space with the necessary conditions. On the other hand, the detection depends on the instrument that measures the properties of the particles. This detection can be done directly or indirectly by the products of the mother particle analyzed.

Firstly, will be explained how to produce a Higgs at the LHC. The main channel for the production of this particle is through gluon fusion mediated by a loop of tops. The cross-section of this process is estimated to be on the order of 1 pb. This involves colliding $10^9$ protons to produce a Higgs. On the other hand, for the detection it is necessary to consider two factors: the decay of the Higgs ($h \to \gamma\gamma$ as an example) and the efficiencies of the detector. With these two consideration, it would take $10^9$ collisions per second (1 GHz) to observe 100 Higgs in a year [19].

How does the LHC obtain a frequency of 1 GHz? A very useful value to understand how it

achieves this is the instantaneous luminosity which in LHC is $\mathcal{L} = 10\frac{Hz}{nb}$ [20]. Multiplying this by the inclusive cross-section of $pp$ which is approximately 1mb gives $\mathcal{L}\sigma = (10\frac{Hz}{nb})(1mb) = 10^8 Hz = 0.1GHz$ [19].

As can be seen, this would allow the Higgs to be detected. The calculation is in the ballpark of the requested value, which was 1 GHz. For BSM signals, which would have a smaller production cross-section, it would be necessary to increase the luminosity.

Thus, can be seen that the LHC generates enormous amounts of information per second. The problem is that it is impossible to store it all, the electronics of current computers do not allow it. That is why a filter is necessary to eliminate irrelevant information. This is the only way that all the data of interest can be processed.

This filter is known as a trigger. It is defined as the characteristic that the event must satisfy to be saved in memory. There are two levels of trigger: the first level is associated with the hardware and the second with the software level.

The main experiments of the LHC are ALICE, LHCb, ATLAS, and CMS, each one having their own set of detectors. The latter two are designed in four parts: the inner tracker system, which is located near the beamline and is responsible for measuring the traces of charged particles; the electromagnetic calorimeter, which mainly measures the energies of electrons and photons; the hadronic calorimeter, which measures the energy of protons and neutrons; and finally, the muon detector. In the following sections, greater detail will be given to each of these parts, linking them to what was worked on in this report.

### 2.2.1 Inner Tracker

The inner tracker system (ID) allows the detector to efficiently measure the trajectory of an energetic charged particle. The range of the quantities of these values that can be measured depending on the efficiency of the ID. If a neutral particle decays here, its decay vertex can be reconstructed; this means that the secondary vertex of the long lived particles can be detected here [6].

### 2.2.2 Calorimeter

The main objectives of a calorimeter are to measure the energy of particles going through it regardless of their charge, reconstruct the spatial location where the energy was deposited and, sometimes, reconstruct the track as well. The interaction of particles with the calorimeter gives

place to a shower of particles that deposit their energy in detectors.

On one hand, the electromagnetic calorimeter (ECAL) is designed to detect electromagnetic showers generated by electrons and photons.

On the other hand, the hadronic calorimeter can measure the above quantities for hadrons, meaning all particles composed of quarks. As before, a shower is generated here, but in this case is hadronic. It should be emphasised that the hadronic shower in this section is due to the inelastic collision of protons with the detector particles, which mostly creates pions [21].

### 2.2.3 Muon detector

The reason why an electron looses its energy in the ECAL is due to the Bremsstrahlung process; the lost energy is inverse to the squared of the mass of the particle.

The muon is 200 times more massive than the electron. As consequence of this difference in the scale of masses, detecting the muon is not feasible evaluating the bremsstrahlung emission [22].

For everything said above, the reduction on energy over distance traveled is achieved due to ionization, a process that causes heavy charged particles to interact with electrons from the materials of the detector and excites or ionizes them.

$$\left(\frac{dE}{dx}\right)^{muons}_{bremsstrahlung} \ll \left(\frac{dE}{dx}\right)^{muons}_{ionization} \tag{23}$$

It is because this limited effect of ionization that the muon can go through a considerable quantity of absorbent material without being observed.

In addition, at the high energies handled in accelerators, the importance of ionization effects with the medium decrease [23].

All these reasons motivate the construction of robust detection chambers outside the calorimeters that measure observables relative to the muons using the curvature of their trajectories under strong magnetic fields.

## 2.3 Reconstructed Quantities at the LHC

The information that the particles carry are left in the detectors as signals; this allows to reconstruct their properties. This quantities are divided in two: observable and geometric quantities.

For this purpose, it is useful to denote that the convention establishes that the $z$ axis indicates the direction of the beam of particles in the detector. Therefore, the transversal components of

are represented by $x$ and $y$.

The above allows us to work with quantities that are invariant under changes in the reference system. Some of the most important are the following.

### 2.3.1 Transverse Momentum

It is defined using the transverse components of the momentum, i.e. $p_x$ and $p_y$. The vector, along with its scalar representation are given below.

$$\vec{p_T} \equiv (p_x, p_y), \qquad p_T \equiv |\vec{p_T}| \tag{24}$$

### 2.3.2 Missing Transverse Energy

Neutrinos don't leave track in the detectors, however, their energetic contribution to events can be significant. As a consequence, a specific quantity for labeling every non-measured energy contribution is defined as **missing transverse energy (MET)**. This is a scalar quantity defined using conservation of momentum and using the analogous concept of **missing transverse momentum**:

$$\vec{\not{p}}_{\mathrm{T}} \equiv -\sum_i \vec{p_{T_i}} \tag{25}$$

Here, $\vec{p_{T_i}}$ equals the transverse momentum of particle $i$ that could be measured; the sum goes over all detected particles. With this, the MET is defined as the following:

$$\not{E}_{\mathrm{T}} \equiv |\vec{\not{p}}_{\mathrm{T}}| \tag{26}$$

### 2.3.3 Invariant Mass

The detection of short-lived particles or those that interact feebly with the detector is achieved by their decay in particles that can be measured. The **invariant mass** reconstructs the mass of the particle of interest and is defined as the following way:

$$m_{objetos} = \left| \sum_{objeto} \sum_i p_i^{\mu} \right|^2 \tag{27}$$

In this equation, the reconstruction is made from the sum of particles that are believed to come from the particle that has decayed.

### 2.3.4 Effective Mass

Let us consider a situation where a resting particle originated from a $pp$ colision is at rest and then decays. If the all the decay products have their momenta in the transverse plane, then it is possible to reconstruct their mass with the **effective mass**:

$$M_{eff} \equiv \sum_i |\vec{p_{T_i}}| + \vec{\not{E}}_{\mathrm{T}} \tag{28}$$

If there is a situation where a particle is longitudinally boosted, this relation will not be precise.

It is also helpful to define variables that give results involving the geometry of the detector in order to locate and classify the particles; the most important are presented below.

### 2.3.5 Rapidity and Pseudorapidity

In order to have a quantity that gives information about how fast a particle moves in the direction of the beam that remains invariant under boost in this direction, the **rapidity** is defined as

$$y = \frac{1}{2} \ln \frac{E + p_z}{E - p_z} \tag{29}$$

Using this definition, we can define **pseudorapidity** $\eta$, a function of the polar angle $\theta$ that varies from $-\infty$ to $\infty$ when $\theta$ changes from 0 to $\pi$, as it is shown in Figure 2. The described relation is represented with the following:

$$\eta \equiv \ln \cot \frac{\theta}{2} \tag{30}$$

When a Taylor expansion around $\theta = \frac{\pi}{2}$ is applied, the above equation turns into this next expression:

$$\eta \approx \frac{\pi}{2} - \theta \tag{31}$$

Pseudorapidity shows how far from the main vertex the particle is located with respect to the beamline.

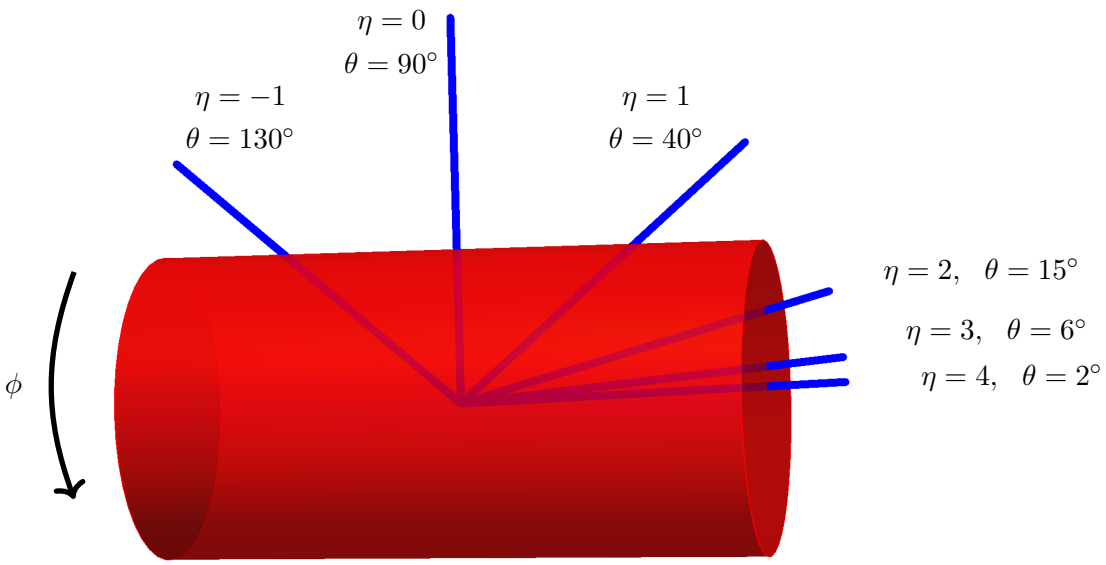


Figure 2: Pseudorapidity $\eta$ goes from $\infty$ a $-\infty$ centered on the collision origin. Azimuth angle $\phi$ twists around the beamline. Figure taken from [19].

### 2.3.6 Azimuth Angle

To complete the description of the position for a particle, it is required to introduce a new concept: **azimuth angle** $\phi$. Its domain, located in the plane orthogonal to the beamline, goes from 0 to $2\pi$ and it indicates the trajectory in a detector. This boost invariant quantity is defined in terms of the transversal components $p_x$ and $p_y$:

$$\phi \equiv \tan^{-1} \frac{p_x}{p_y} \tag{32}$$

### 2.3.7 Angular Separation

The geometric quantities described above give a calculation that depends on the system of reference; therefore, to obtain an invariant quantity, the **angular separation $\Delta\mathbf{R}$** is used. This amount relates the geometric position of two particles and it is boost invariant. The definition uses the differences of rapidity and azimuth angle and it is described as the following:

$$\Delta R = \sqrt{(\Delta y)^2 + (\Delta \phi)^2} \tag{33}$$

## 2.4 Displaced Vertex and heavy neutrino

In collider physics, a displaced vertex refers to the location where a particle decay occurs away from the primary collision point. This can occur when particles with a relatively long lifetime, such as heavily flavored mesons or long-lived neutral particles, are produced in high-energy collisions at particle accelerators [24, 25].

Displaced vertices are used in a wide range of physics analyses, including searches for new particles BSM (they can be used in the search of long-lived neutralino in supersymmetric models) and measurements of the properties of known particles [26].

Additionally, heavy neutrinos could potentially decay into other particles that are easier to detect, such as electrons or muons. When these neutrinos are lighter than the $W$ boson, have small mixings and are produced via neutral currents that can be measured at the LHC, such as the decay of the $Z$ or the Higgs, they can be long live particles. Thus, the decay process could result in a displaced vertex that can be detected in the ID.[7, 15, 27].

## 2.5 Jets

The parton shower caused by the hadronization of quarks and gluons causes these particles to multiply, giving as final result a stream of quarks and gluons. These final state particles, however, come from one single parton, so it is expected to find information that relates the final state hadron with the original parton.

In order to connect these final hadrons to the expected parton, the concept of Jet is created. As the particles move away from the interaction point, they are collimated into a narrow cone by the strong force, resulting in a jet of particles.

The properties of a jet, such as its energy, momentum, and substructure, can be measured experimentally by detecting and reconstructing the individual particles that make up the jet. The way of doing this, and the results provided, vary depending on the reconstruction algorithm that is used. In the following section, the to go algorithm for this task in the LHC is presented.

### 2.5.1 The anti-$k_t$ jet clustering algorithm

Born as an extension of the $k_t$ and Cambridge/Aachen algorithm, the anti-$k_t$ algorithm began with a redefinition of the distance measures, where we have the desired method when $p = -1$:

$$d_{ij} = \min(k_{ti}^{2p}, k_{tj}^{2p}) \frac{\Delta_{ij}^2}{R^2}\,, \tag{34a}$$

$$d_{iB} = k_{ti}^{2p}\,, \tag{34b}$$

Here, $\Delta_{ij}^2 = (y_i - y_j)^2 + (\phi_i - \phi_j)^2$ and $k_{ti}$, $y_i$ and $\phi_i$ are respectively the transverse momentum, rapidity and azimuth of particle $i$.

The preference of this procedure over others relies on various factors, but the main one is that the soft particles do not modify the construction of the jet shapes; ergo, the algorithm remains robust under alteration due to soft radiation [28].

For the above to be accomplished, the equations in 34 denote that these soft particles tend to cluster with hard ones, meaning high transverse momenta, before doing it with themselves. In this situation, with no other hard particle around a distance of $2R$, the shape of the jet is a perfect cone. If, however,there is another hard particle, the shape will not be perfectly cone-shaped. The Figure 3 represents the execution of this algorithm.

# 3 Methods: Description of software

Once the Lagrangian of the theory that one wants to study is obtained, it goes through a process where the information is extracted, manipulated, and used in collider simulations.

The identification of the lagrangian parameters and interactions is achieved with `SARAH`, a software based in Mathematica that generates compilable modules and a Universal FeynRules Output (UFO).

First of all, the compilable modules represent a source code to run in `SPheno`, which is a program that calculates, mainly, two things: the mass matrix where the information of the spectra and mixing is found; and the decay partial widths, where the total width $\Gamma$ and branching ratios are located. The output file generated can be taken as a `param_card.dat` input for `MadGraph5_aMC@NLO`.

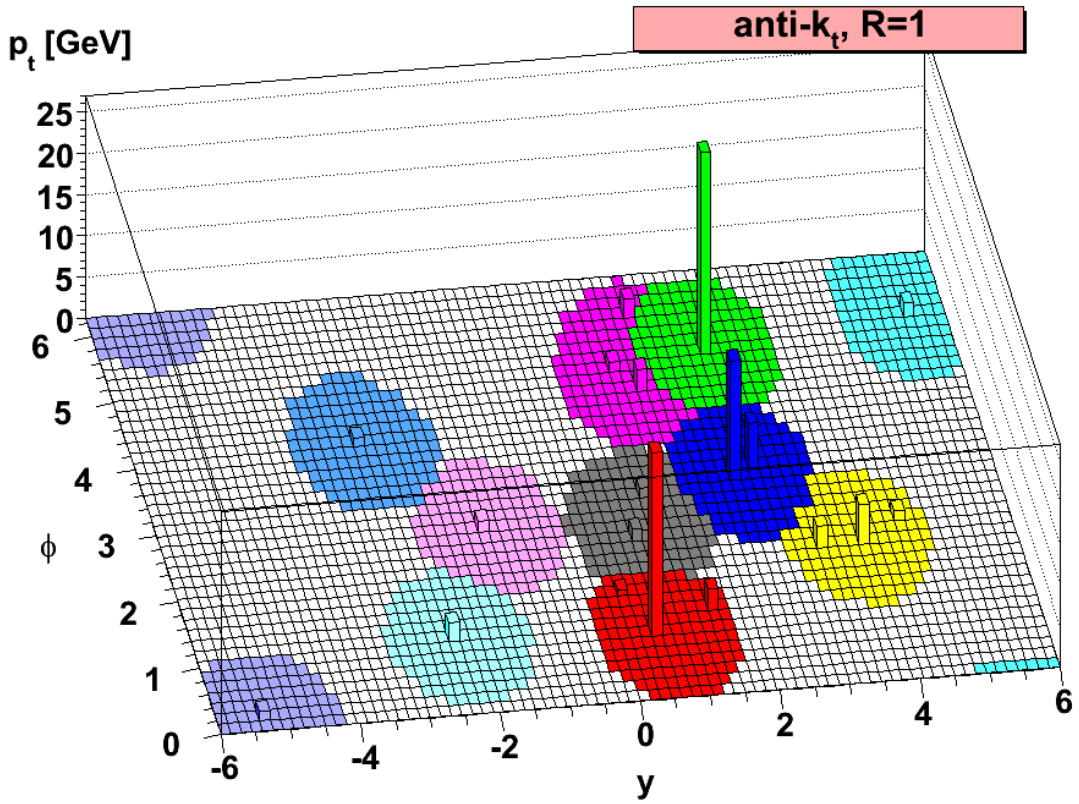


Figure 3: Jet cone structure provided by the anti-$k_t$ jet clustering algorithm. Figure taken from [28]

## 3.1 MadGraph5_aMC@NLO

`MadGraph5_aMC@NLO` is a Monte Carlo particle collider simulator that, using the output files before mentioned, calculates the partonic level cross section. With this information, events from hadron colliders, like the ones in LHC, or linear colliders, like the future International Linear Collider can be generated using SM or BSM. The output generated here goes as input for `Pythia8`. This software generates the parton shower and the hadronization, described in  Jets. The algorithm output from `Pythia8` is used as input for `Delphes`.

### 3.1.1 Delphes

`Delphes` can achieve a simulation of the detectors from the colliders detailed in Section 2.2. With this, the reconstructed data for jets, electrons, muons, taus and isolated photons are accessible [29]. As a consequence, this process also reconstructs the missing energy.

## 3.2 FastJet

This is a software used to implement the Jet Clustering Algorithm. `FastJet` works as a library that is compiled so that the event information stored in the output files from `MadGraph5_aMC@NLO` contain data from their corresponding jet reconstruction [30]. For this analysis, the implemented algorithm in `FastJet` is the anti-$k_t$.

## 3.3 MadAnalysis 5

When conducting an experiment, it is important to distinguish between the signal and the noise, which is also known as background. The signal is made up of the final states of the process being studied, while the background is made up of similar final states that can be either reducible or irreducible.

Reducible background is when the final state of the particles is similar, often due to issues with the detector. By improving the detectors, it is possible to reduce this type of background.

Irreducible background happens when the final states that are measured have the same particle content as the final state of interest, making them indistinguishable from each other. It is due to this noise that it is useful to characterize the signal and background regions associating them intervals for the measurements of observable described in 2.2.

However, there will always be some noise present in the signal region. But, if the background has been properly characterized, it is possible to estimate the contamination of this signal region through extrapolation.

MadAnalysis 5 is a C++-based framework for analyzing particle collisions, and it includes a feature called 'cuts' that are similar to experimental filters. The cuts help to filter events and define the signal region based on specific features that an event must satisfy [31, 32]. If an event does not meet these requirements, it is considered part of the background region. The efficacy of these cuts can be verified using a file called 'cutflow'.

This software provides two modes of analysis: Normal Mode and Expert Mode. Normal Mode consists of a Python interface that allows for the extraction of information using preimplemented analysis and results can be obtained quickly. Expert Mode, on the other hand, has a C++ interface that enables the customization of the analysis through the selection of cuts and plotted histograms. For this work, Expert Mode was used.

`MadAnalysis 5` allows for analysis at the two levels mentioned in the previous section: Monte Carlo Part and Reconstructed. Since the information collected by the detector simulation is far

from complete, implementing both levels for an event of interest is useful.

This urge to compare data in these two levels is the main motivation why the information from FastJet and displaced vertices is required in Monte Carlo, since, for now, it is only available in the Reconstructed mode. In the following section, the methods on how this was achieved are described.

# 4 Methods: Execution of software

The following instructions will contain the description of the steps used to get the results that meet the objectives. The files compiled for the Fastjet and Displaced Vertex part will be accessible in the following github repository: https://github.com/walterrq/dv_fastjetImp.git.

## 4.1 Methods for Displaced Vertices in Monte Carlo

For the implementation of displaced vertices at Madgraph level, two procedures were necessary: first, the decay width was changed from a value of $3 \cdot 10^{-12}$ GeV to $3 \cdot 10^{-16}$ GeV. The first case was expected to have no displaced vertices, while for the second one, it was expected to have them. This was done in the `param_card.dat` located in `MG5_aMC_v3_4_1/lhcevent/Cards`. The second procedure consists of running the code for event generation. We must make sure that in the Madgraph `run_card.dat` we have the "time of flight option" activated:

```
0.0 = time_of_flight ! threshold (in mm) below which the invariant livetime
↪  is not written (-1 means not written)
```

At the `MadAnalysis 5` level, the implementation was direct. This was done in a usual `MadAnalysis 5` installation with a version from 2017 onwards. For this case, we can take as reference the github repository: https://github.com/MadAnalysis. First we access the file `MCParticleFormat.h` which is located in:

```
MadAnalysis5/tools/SampleAnalyzer/Commons/DataFormat/
```

Inside, we look for a function that returns as output the vertex where a "daughter" of the LLP was produced. For different versions of `MadAnalysis 5` this function has different syntax. Normally, the name of the function is sufficiently explicit for it to be easily detected. In our case, we used the version of `MadAnalysis 5` from the year 2021 and it had the function `MALorentzVector& decay_vertex()` that exactly satisfies the definition given earlier.

The syntax of the function coincides with the mentioned repository which is from the year 2022. Finally, this function is implemented in expert mode using a `.cpp` file. This allows the implementation of the corresponding histograms that will be specified in the Section 5.1.

## 4.2 Methods for FastJet execution in Monte Carlo

In order to obtain the information of Jets in MC level, a manual FastJet activation is needed. This implies the proper linking of FastJet libraries and use of its instances and variables.
In the first place, the linking, as detailed on the `MyAnalysis.cpp` file for FastJet execution, needs for the libraries to be copied to the same level as the `Build` folder. Once this was done, they had to be called with the following structure:

```
#include "fastjet/PseudoJet.hh"
#include "fastjet/ClusterSequence.hh"
#include "fastjet/Selector.hh"
```

It is also needed to specify the use of these libraries. This is done with the next line:

```
using namespace fastjet;
```

In the second place, the linking requires to modify the `Makefile` to include the FastJet linkers and requirements before building. For the linking option, the instruction would indicate the next:

```
LIBFLAGS += -lprocess_for_ma5 $(shell
↪ $(MA5_BASE)/tools/SampleAnalyzer/ExternalSymLink/Bin/fastjet-config
↪ --libs) -lEG
```

For the requirement, as specified on the `Makefile` file, the instruction has to be with `libfastjet_for_ma5.so` instead of the `libfastjet.so` because the latter was not specially modified for running in `MadAnlysis 5`:

```
REQUIRED3 = $(MA5_BASE)/tools/SampleAnalyzer/Lib/libfastjet_for_ma5.so
```

Once all the above is set correctly, one has to make sure that the FastJet syntax is used properly. This has to be ensured specially because, along the code, variables from MA5 and FastJet will be needed, and a variable set with one library can not be used with other variable initially defined with other library in one same function, as required for computing the $\Delta R$. To make this possible, the syntax can be found in [30].

# 5 Results

## 5.1 Displaced Vertex in Monte Carlo

Now we will focus on the results associated with Displaced Vertex in Monte Carlo. As a first approach, we want to obtain the four vectors that give the coordinates of the displaced vertex for the heavy neutrino ($N_4$). The values of this four-vector will depend on the decay width of the heavy neutrino. These two quantities are inversely proportional: if the width decay is bigger, then the distance of the decay vertices for the $N_4$ particle will be reduced. In the limit where the width is sufficient largely, it will be a promptly decaying neutral lepton.

Firstly, we will plot the displaced vertex for a decay width equal to $3 \cdot 10^{-12}$ GeV for the heavy neutrino. This is shown in Figure 4 for the time and $x$ variables. The interval of the bins is 5 nanoseconds and 5 mm respectively.

In general terms, for the mentioned width, it was expected that the values of the decay vertex will be low. This means that the case of the position will have a very small decay vertex values in the millimeter order. For this reason, the result has a very low mean close to zero in the case of time and of a few millimeters in the position.

The given histograms shows that the value of the displaced vertices (DV) is very low. As is observed for the time variable, the peak has 3200 events in the first interval that goes from 0 to 5 nanoseconds. On the other hand, for the $x$ variable, a lower peak with only 1800 events and more spread values is seen. The tendency for these two variables is to have low values; however, the problem with this is that, as a first approach for using the DV in MC, is a questionable result. This is because sometimes the information of the DV is not well filled or linked to the programs. In this scenario, the closeness to zero values could be a default result for the data. This does not give a reliable result for the DV application in MC. For this reason, to confirm if the data and functions of `MadAnalysis 5` are being well implemented for displaced vertices, we change the decay width to a lower value. As it was mentioned before, this will allow us to have bigger values for the DV. In this case, we selected a value of $3 \cdot 10^{-16}$ GeV that would allow us to have DV of the order of the millimeters. It is expected to have a more spread-out value for the DV with a higher mean. As it was done before, we plot the time and $x$ variables for the decay width with the value $3 \cdot 10^{-16}$ GeV. This can be seen in Figure 5 with the same value for the intervals of the bins (5 nanoseconds and 5 mm). The provided histogram shows the results that were expected. In the case of the time variable, the mean increased from 0.74 to 474.8. In this new case, it can not be

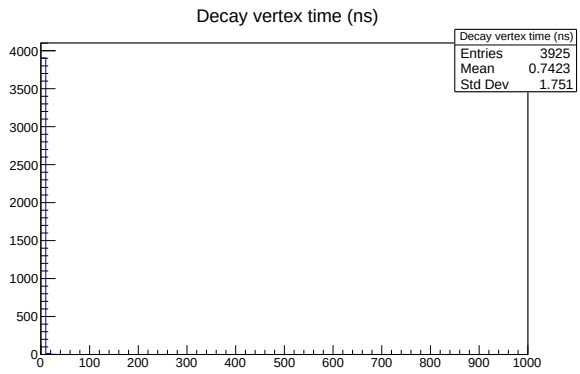


(a) Decay vertex for the time variable for the $N_4$

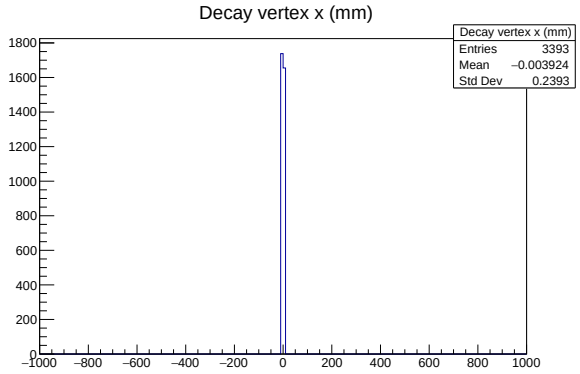


(b) Decay vertex for the x variable for the $N_4$

Figure 4: Decay vertices for decay width equal to $3 \cdot 10^{-12}$ GeV

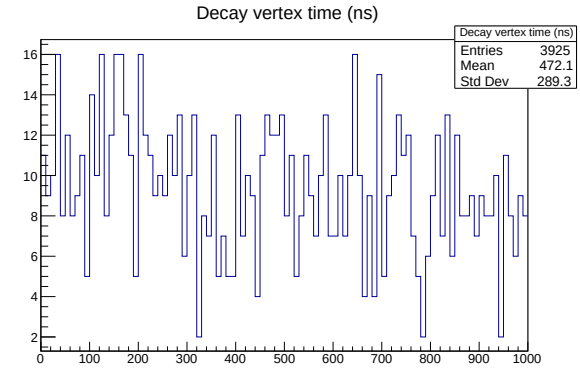


(a) Decay vertex for the time variable for the $N_4$

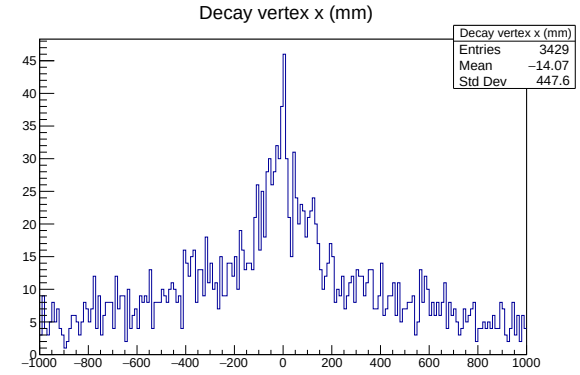


(b) Decay vertex for the x variable for the $N_4$

Figure 5: Decay vertices for decay width equal to $3 \cdot 10^{-16}$ GeV

observed a peak in any value. Instead, there is a more homogenic distribution along the time axe. A different view is for the case of the $x$ variable. In this histogram, a peak in the center, equally to the case where the decay is $3 \cdot 10^{-12}$ GeV, can be seen. The big difference is that this peak is in the order of $10^1$. Meanwhile, in the other case, it was of the order $\cdot 10^3$. Moreover, another difference is that the distribution is more spread out with a big standard deviation (447.6) as can be seen in Figure 5.

This final result allows us to verify the sensitivity of the simulation to changes in decay widths. Additionally, with this is possible to make a cross-check the implementation of DV in `MadAnalysis 5`.

## 5.2 FastJet execution in Monte Carlo

Once we were able to link FastJet with `Madanalysis 5`, one way to check the correct execution of these two programs is to compare the pions to the jets variables. Due to the fact that the main composition of the jets are pions, as explained before, it is expected for them to have similar properties.

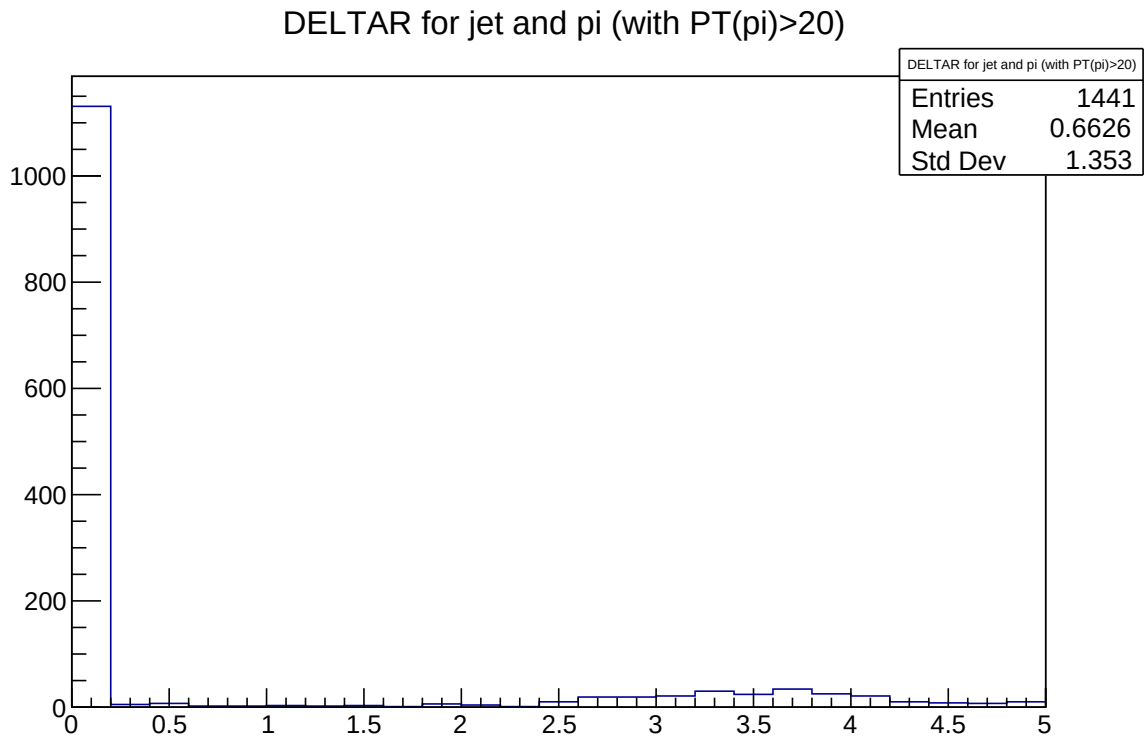


Figure 6: $\Delta R$ for leading pion and leading jet plot for Monte Carlo.

For the first analysis, the $\Delta R$ between the leading jet and leading pion was plotted. This relation is shown in the Figure 6. The anti-$k_t$ jet clustering algorithm forms its trajectory through the

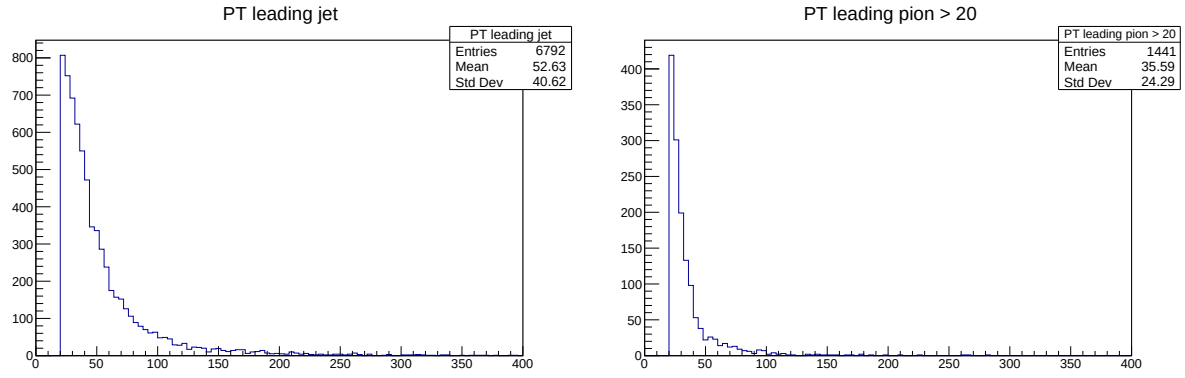


(a) Transverse momentum for leading jet in MC. (b) Transverse momentum for leading pion in MC.

Figure 7: Transverse Momentum plot

most energetic component of the jet. In most cases, it is expected for this highest energy particle to be a pion. Since the leading pions are inside the jet cone, their positions in the detector would be expected to be similar. A quantitative way to measure this closeness is through a small value $\Delta R \to 0$.

As can be observed in Figure 6 most of the events have the $\Delta R$ of the leading pion and leading jet close to zero. As explained before, this peak in zero was expected because the trajectories of this two objects are similar. The mean has a value of 0.66 with an standard deviation of 1.3. The high values can be explained because of three factors: First of all, in some cases, the pion will not be the most energetic particle. Second of all, the initial state radiation that comes from the gluon fusion can make some pions or jets have opposite trajectories in the transverse plane. Third of all, there might be two jets in an event where the jet containing the leading pion is not the most energetic; this can happen if the jet without the leading pion has many more energetic particles than the other jet.

Additionally, to verify the correspondence between the jet and the pion, the transversal momentum of the jet and the pion are plotted in Figure 7 with a cut of 20 GeV. This plot shows that the number of events with a jet passing the cut is greater than the number of events with at least a pion passing the cut. This is because not only pions generate jets, but more particles are involved in their generation. In addition, to find the transverse momentum of the jet, the modules of all the constituents must be added. In this way, there will be a higher value of transverse momentum and therefore not as many events will be lost after the 20 GeV cut.

# 6 Conclusion

In the present report, we aimed to modify the `MadAnalysis 5` program to encode information about the production point of the displaced vertex at the Monte Carlo level. This was achieved as seen the histogram 5, which shows the distribution of the position and time of the displaced vertex after the decay of the heavy neutrino $N_4$. To do this, it was necessary to change the decay width from a value of $3 \cdot 10^{-12}$ GeV to $3 \cdot 10^{-16}$ GeV and also to access the necessary `.h` files to find the correct functions. For the decay width value of $3 \cdot 10^{-16}$ GeV, the expected behavior of a displaced vertex was observed, as the values were distributed more sparsely along the axis. Meanwhile, in the case of $3 \cdot 10^{-12}$ GeV, the data was collapsed at zero, so it did not allow to discern if the implementation was being applied correctly. Furthermore, in line with the second objective, we managed to execute `FastJet` externally in parallel with `MadAnalysis 5` to achieve a jet assignment. This was accomplished by linking the `Fastjet` libraries and editing the `Makefile` as specified in 4.2. To verify that the implementation has been carried out correctly, two crosschecks were performed. On the one hand, we verified that the value of $\Delta R$ between the leading jet and the leading pion was close to zero. This was corroborated in Figure 6. On the other hand, a comparison was also made between the transverse momentum of the leading pion and the leading jet. The distributions had similar behaviors, and the reason for the difference in events was detailed.

## References


[1] P. Minkowski, "$\mu \to e\gamma$ at a rate of one out of 109 muon decays?," *Physics Letters B*, vol. 67, no. 4, pp. 421–428, 1977.

[2] M. Gell-Mann, P. Ramond, and R. Slansky, "Complex Spinors and Unified Theories," *Conf. Proc. C*, vol. 790927, pp. 315–321, 1979.

[3] T. Yanagida, "Horizontal gauge symmetry and masses of neutrinos," *Conf. Proc. C*, vol. 7902131, pp. 95–99, 1979.

[4] R. N. Mohapatra and G. Senjanović, "Neutrino mass and spontaneous parity nonconservation," *Phys. Rev. Lett.*, vol. 44, pp. 912–915, Apr 1980.

[5] O. Sawada and A. Sugamoto, eds., *Proceedings: Workshop on the Unified Theories and the Baryon Number in the Universe: Tsukuba, Japan, February 13-14, 1979*, (Tsukuba, Japan), Natl.Lab.High Energy Phys., 1979.

[6] A. Donini, P. Hernández, J. López-Pavón, M. Maltoni, and T. Schwetz, "The minimal 3 2 neutrino model versus oscillation anomalies," *Journal of High Energy Physics*, vol. 2012, jul 2012.

[7] J. Jones-Pérez, J. Masias, and J. D. Ruiz-Álvarez, "Search for long-lived heavy neutrinos at the LHC with a VBF trigger," *The European Physical Journal C*, vol. 80, jul 2020.

[8] M. Fukugita and T. Yanagida, *Physics of neutrinos and applications to astrophysics*. Theoretical and Mathematical Physics, Berlin, Germany: Springer-Verlag, 2003.

[9] P. Hernández, J. Jones-Pérez, and O. Suarez-Navarro, "Majorana vs pseudo-dirac neutrinos at the ILC," *The European Physical Journal C*, vol. 79, mar 2019.

[10] R. Alonso, M. Dhen, M. B. Gavela, and T. Hambye, "Muon conversion to electron in nuclei in type-i seesaw models," *Journal of High Energy Physics*, vol. 2013, jan 2013.

[11] A. Atre, T. Han, S. Pascoli, and B. Zhang, "The search for heavy majorana neutrinos," *Journal of High Energy Physics*, vol. 2009, pp. 030–030, may 2009.

[12] M. Blennow, E. Fernandez-Martinez, J. Lopez-Pavon, and J. Menéndez, "Neutrinoless double beta decay in seesaw models," *Journal of High Energy Physics*, vol. 2010, jul 2010.

[13] A. Ibarra, E. Molinaro, and S. T. Petcov, "Low energy signatures of the tev scale seesaw mechanism," *Phys. Rev. D*, vol. 84, p. 013005, Jul 2011.

[14] A. Pilaftsis, "Radiatively induced neutrino masses and large higgs-neutrino couplings in the standard model with majorana fields," *Zeitschrift fr Physik C Particles and Fields*, vol. 55, pp. 275–282, jun 1992.

[15] A. M. Gago, P. Hernández, J. Jones-Pérez, M. Losada, and A. M. Briceño, "Probing the type 1 seesaw mechanism with displaced vertices at the LHC," 2015.

[16] "LHC Machine," *JINST*, vol. 3, p. S08001, 2008.

[17] G. Aad *et al.*, "Observation of a new particle in the search for the standard model higgs boson with the ATLAS detector at the LHC," *Physics Letters B*, vol. 716, pp. 1–29, sep 2012.

[18] S. Chatrchyan *et al.*, "Observation of a new boson at a mass of 125 GeV with the CMS experiment at the LHC," *Physics Letters B*, vol. 716, pp. 30–61, sep 2012.

[19] M. D. Schwartz, "Tasi lectures on collider physics," 2017.

[20] O. S. Bruning, "LHC luminosity and energy upgrade: A feasibility study," 12 2002.

[21] L. Cerrito, *Electromagnetic and Hadronic Showers: Calorimeters*, pp. 171–185. Cham: Springer International Publishing, 2017.

[22] M. Livan and R. Wigmans, *Interactions of Particles with Matter*, pp. 31–51. Cham: Springer International Publishing, 2019.

[23] R. L. Workman and Others, "Review of Particle Physics," *PTEP*, vol. 2022, p. 083C01, 2022.

[24] S. Jana, N. Okada, and D. Raut, "Displaced vertex and disappearing track signatures in type-iii seesaw," 2019.

[25] F. G. Celiberto, "High-energy emissions of light mesons plus heavy flavor at the LHC and the forward physics facility," *Physical Review D*, vol. 105, jun 2022.

[26] A. Sirunyan *et al.*, "Search for long-lived particles decaying to jets with displaced vertices in proton-proton collisions at $\sqrt{s} = 13$ TeV," *Physical Review D*, vol. 104, sep 2021.

[27] S. Antusch, E. Cazzato, and O. Fischer, "Sterile neutrino searches via displaced vertices at LHCb," *Physics Letters B*, vol. 774, pp. 114–118, nov 2017.

[28] M. Cacciari, G. P. Salam, and G. Soyez, "The anti-ik/isubit/i/subjet clustering algorithm," *Journal of High Energy Physics*, vol. 2008, pp. 063–063, apr 2008.

[29] J. de Favereau, , C. Delaere, P. Demin, A. Giammanco, V. Lemaître, A. Mertens, and M. Selvaggi, "DELPHES 3: a modular framework for fast simulation of a generic collider experiment," *Journal of High Energy Physics*, vol. 2014, feb 2014.

[30] M. Cacciari, G. P. Salam, and G. Soyez, "FastJet user manual," *The European Physical Journal C*, vol. 72, mar 2012.

[31] E. Conte, B. Fuks, and G. Serret, "MadAnalysis 5, a user-friendly framework for collider phenomenology," *Computer Physics Communications*, vol. 184, pp. 222–256, jan 2013.

[32] E. Conte and B. Fuks, "Confronting new physics theories to LHC data with MADANALYSIS 5," *International Journal of Modern Physics A*, vol. 33, p. 1830027, oct 2018.